Topological states in a two-dimensional metal alloy in Si surface: BiAg/Si(111)-4×4 surface

Xiaoming Zhang, Bin Cui, Mingwen Zhao, and Feng Liu

Phys. Rev. B **97**, 085422 — Published 16 February 2018

DOI: 10.1103/PhysRevB.97.085422

Topological States in a 2D Metal Alloy in Si Surface: BiAg/Si(111)-4×4 Surface

Xiaoming Zhang,[1,2,3] Bin Cui,[2,3] Mingwen Zhao[3*] and Feng Liu[2,4*]

[1] *Institute for Advanced Study, Tsinghua University, Beijing 100084, China*
[2] *Department of Materials Science and Engineering, University of Utah, Salt Lake City, Utah 84112, USA*
[3] *School of Physics and State Key Laboratory of Crystal Materials, Shandong University, Jinan, Shandong 250100, China*
[4] *Collaborative Innovation Center of Quantum Matter, Beijing 100084, China*

*E-mail: fliu@eng.utah.edu, zmw@sdu.edu.cn

ABSTRACT

Bridging topological state with conventional semiconductor platform offers an attractive route towards future spintronics and quantum device applications. Here, based on first principles and tight-binding calculations, we demonstrate the existence of topological states hosted by a two-dimensional (2D) metal alloy in Si surface, the BiAg/Si(111)-4×4 surface, which has already been synthesized experimentally. It exhibits a topological insulating state with an energy gap of 71 meV (~819 K) above the Fermi level and a topological metallic state with *quasi*-quantized conductance below the Fermi level. The underlying mechanism leading to the formation of such non-trivial states is revealed by analysis of the "charge-transfer" and "orbital-filtering" effect of Si substrate. A minimal effective tight-binding model is employed to reveal the formation mechanism of the topological states. Our finding opens new opportunities to detect topological states and measure its quantized conductance in a large family of 2D surface metal alloys, which have been or are to be grown on semiconductor substrates.

INTRODUCTION

With the feature of quantized spin Hall conductance (SHC) [1,2], the topological states of two-dimensional (2D) materials were extensively studied due to their fundamental interest and potential applications ranging from spintronics to quantum computation. While the prediction of topological edge states has been well developed [3-5], to date only two systems of HgTe/CdTe and InAs/GaSb quantum well [6,7], have been confirmed with nontrivial edge states of quantized conductivity but having too small a band gap.

Earlier studies have shown topological edge states of Bi on non-semiconducting substrates, such as Bi(111)/Bi_2Te_3 [8-10], Bi(110)/Graphite [11], and Bi(111)/Sb [12], but with unwanted hybridization between the overlayer topological states and substrate trivial states. To overcome this problem, an interesting idea was proposed to take advantage of the so-called "orbital-filtering" effect of substrate [13], so that topological state can be induced by depositing metal, such as Bi honeycomb lattice on semiconductor surface, such as Si [13], SiC [14] or Ge [15] surface, without hybridization. The resulting large non-trivial gap and the conductive edge state has been experimentally confirmed on SiC surface recently [14]. The topological edge state has also been theoretically predicted and experimentally confirmed in a 2D superconductor overlayer in FeSe/$SrTiO_3$(001) [16], which offers an intriguing platform to study topological superconducting states. However, all these experiments are based on spectroscopy measurements without showing the quantized edge conductivity. The challenging is largely due to a lack of experimental samples with large single surface domain of a perfect metal overlayer. Therefore, the search for 2D topological states continues, especially bridging topological state with conventional semiconductor platform to realize topological states at high temperature is of great interest.

Taking a known experimental example of BiAg alloy on Si(111)-4×4 surface (see Fig. 1a) [17], here we show that the BiAg/Si(111)-4×4 surface has four topologically non-trivial bands stemming from the p_{xy} orbitals of Bi atoms, which are well decoupled from other states, attributed to the charge transfer and orbital-filtering effect of silicon substrate. A minimal effective tight binding (TB) model on a honeycomb lattice is employed to explain the existence of these topological states. Specifically, the topological insulating (TI) state above the Fermi level exhibits a SHC of $-2\times e/4\pi$ within the non-trivial gap of ~71 meV, while that of the topological metallic (TM) state below the Fermi level is mixed with trivial metallic states but still shows a finite width of quantized conductance plateau up to ~50 meV. Our findings suggest that the common 2D surface metal alloys on semiconductors provide a viable family of candidate materials for searching large gap topological states with robust quantized conductance plateau.

METHOD AND COMPUTATIONAL DETAILS

The electronic and topological properties of BiAg/Si(111)-4×4 surface were calculated using Vienna *ab initio* simulation pack (VASP) [18,19] and WANNIER90 [20] within the framework of density functional theory (DFT). Generalized gradient

approximation in the form of Perdew-Burke-Ernzerhof [21] and projector-augmented-wave potentials with the energy cutoff of 500 eV [22] were respectively used for describing the electron-electron and electron-ion interactions. Structural optimizations were performed using a conjugate gradient method on a 3×3×1 Monkhorst-Pack sampling until the remnant force on each atom was less than 0.01 eV/Å, while a dense Gamma-centered sampling (6×6×1) is employed for charge density calculations and establishing the maximally localized Wannier functions (MLWFs).

RESULTS AND DISCUSSION

The top view of BiAg/Si(111)-4×4 surface is displayed in Fig. 1a, which is prepared by depositing about one monolayer Ag onto the mixed Si(111) α-$\sqrt{3}\times\sqrt{3}$ /β-$\sqrt{3}\times\sqrt{3}$ -Bi surface followed by annealing at ~250 °C [17]. One unit-cell of BiAg/Si(111)-4×4 surface has seven bismuth atoms and twenty silver atoms. Besides a single Bi atom located at T_1 site, other Bi atoms form two triangles located over T_4 and H_3 sites. Hence, we name the three types of bismuth as Bi@T_1, Bi@T_4, and Bi@H_3, whose positions can be seen more clearly from Fig. S1 [23]. The Bi@T_4 and Bi@H_3 constructs a perfect Ruby lattice pattern [24], which is highlighted in Fig. 1a. The outmost Si atoms of the top bilayer can also be distinguished through the number of its nearest Bi or Ag atoms.

Figure 1b shows the calculated electronic band structures of BiAg/Si(111)-4×4 surface without considering spin-orbit coupling (SOC), and one clearly sees four bands near the Fermi level which are well decoupled from other bands. In addition to the quadratic points emerging at the Γ point, band crossing takes place along the path from Γ to M point, while no degeneracy (Dirac point) existing at K point. By plotting the charge density distribution of the four isolated bands in Fig. 1c, we conclude that these bands stem mainly from the p_{xy} orbitals of Bi@T_4 and Bi@H_3, while the contributions from other atoms are almost negligible except the p_z orbitals of the Si atoms with three nearest Ag atoms. Notably, the tiny different charge density isosurfaces of Bi@T_4 and Bi@H_3 imply that they are not exactly equivalent due to the substrate effect, which breaks the inversion symmetry so that no Dirac point forms between the two middle bands at K point. The absence of any electronic states from Ag atoms around the Fermi level can be attributed to the significant charge transfer from the BiAg alloy to silicon substrate, as shown in Fig. 1d. Furthermore, the increased electronic density at the interface indicates bond formation, particularly the formation of Bi-Si bonds that have pushed the p_z orbital of Bi atoms away from the Fermi level. This in turn enables the isolation of p_{xy} bands near the Fermi level to be well decoupled from other electronic sates. Such mechanism is similar to Bi honeycomb lattice on a semiconductor substrate [13]. To confirm this, we performed a computational experiment of calculating the band structure of isolated BiAg alloy without substrate (as a hypothetical model system), as shown in Fig. S2 [23]. In addition to the states arising from the Bi p_{xy} orbitals, one can clearly see the metallic

states dominated by Ag atoms and p_z orbital of Bi atoms around the Fermi level, which were removed by the "orbital-filtering" and "charge-transfer" effect of Si substrate.

Taking the SOC into account, the degeneracy at quadratic points and band crossing points are lifted, with significant spin splitting in eight bands, as shown in Fig. 2a. We notice a large SOC energy gap of ~71 meV is opened up above the Fermi level, and new degenerate points (Dirac cone) are formed at the six corners of the first BZ. Here we should point out that the Dirac cone is not protected by symmetry since a weaker SOC strength will destroy it (Fig. S3) [23]. Actually, the gap closing at K point between the two middle bands is the critical points of phase transition that we will show below. The Fermi surface contour is plotted in Fig. 2b, which illustrates highly anisotropic properties, consistent with the anisotropic dispersions of the four isolated bands near the Fermi level.

Spin polarization in x, y, and z direction ($\langle s_x(\vec{k})\rangle$, $\langle s_y(\vec{k})\rangle$, $\langle s_z(\vec{k})\rangle$), defined as $\langle s_\alpha(\vec{k})\rangle = \langle \varphi(\vec{k})|\sigma_\alpha|\varphi(\vec{k})\rangle$, ($\alpha$ = x, y, z) [25], in the Fermi surface contour were calculated to show the spin texture in Fig. 2c. In addition to the nonzero spin polarization in x and y directions, $\langle s_z(\vec{k})\rangle$ has the same order of magnitude as $\langle s_{x/y}(\vec{k})\rangle$ and hence cannot be neglected. Based on the Hamiltonian of extrinsic SOC $\hat{H}_{SOC} \propto \boldsymbol{\sigma}\cdot(\nabla V \times \hat{\mathbf{p}})$, it is easy to show that the nonzero $\langle s_{x/y}(\vec{k})\rangle$ components stem from the out-of-plane potential energy gradient due to the breaking of inversion symmetry in a surface, while the out-of-plane spin polarization is induced by in-plane potential energy gradient contributed mainly by surface BiAg alloy (Fig. S4 [23]), in which the surrounding Ag atoms played a significant role. Considering the nonzero $\langle s_z(\vec{k})\rangle$ is always accompanied by anisotropic Fermi surface contours without a perfect circular shape [26], one can understand that the surrounding Ag atoms have modified the dispersions of the four bands by affecting the electron hopping between the p_{xy} orbitals of Bi@T_4 and Bi@H_3.

In order to further reveal the above mechanism, we construct a minimal effective TB model by placing both of p_x and p_y orbitals on a honeycomb lattice (Fig. 3a), where the second-neighbor hopping parameters, t^1 and γ, can be regarded as the electron hopping induced by the surrounding Ag atoms. The Hamiltonian is written as $H=H_0+H_{SOC}$ and details can be found in the supplemental materials [23]. Diagonalizing the Hamiltonian of H_0 in reciprocal space, we obtain four bands plotted in Fig. 3b, which show the exactly same features as the isolated four bands of BiAg/Si(111)-4×4 surface shown in Fig. 1b, including the quadratic point, bands crossing point, and the absence of the Dirac point resulted from the different onsite energies attained by the orbitals in the different sub-lattices. When considering intrinsic SOC [27, 28], all the degenerate points are lifted and new Dirac points

emerge at the six corners of first BZ (Fig. 3c), similar to the above DFT results. Then we examine the band evolution with respect to the decrease of the electron hopping parameters (t^1, γ), to simulate the effect of decreasing the perturbations of surrounding Ag atoms, as plotted in Fig. S5a, S5b, and S5c [23]. One can clearly see that the four bands (Fig. 3c) gradually evolve into the well-known four topological bands composing of two Dirac bands sandwiched by two flat bands (Fig. 3d) [27]. This indicates that the perturbations of surrounding Ag atoms only distort the shape (i.e., dispersion) of Dirac and flat bands but without closing or reopening any gap, so that the topology of all four bands remains intact. Thus, the fours bands in Fig. 3c and 3d share the same topological property.

Next we investigate the topological properties of BiAg/Si(111)-4×4 surface. We first confirm the existence of non-trivial topological edge states, which can be directly compared with the experimental results of spectroscopic techniques [8-12,14,16]. The plane-averaged charge density along *z*-axis (Fig. S6 [23]) indicates the formation of 2D electron gas at the surface of silicon substrate. Hence a recursive strategy is employed to construct the edge Green's function of *semi*-infinite lattice from MLWFs [29], which were established by defining the p_{xy} orbitals on honeycomb lattice to generate the initial guess for the unitary transformations. The Wannier-interpolated band structure is plotted in Fig. 4a, which shows good agreement with the DFT bands (Fig. 2a). The local density of states (LDOS) calculated from the edge Green's function are plotted in Fig. 4b. One can clearly see two topological Dirac-like edge states respectively located at the energy window above and below the Fermi level, indicating that some finite amount of *n*-doping or *p*-doping can turn the system into either a TI or a TM. Next, we calculated the topological invariants to confirm the non-triviality of bands. By means of time-reversal polarization [30], we track the *largest gap* between the adjusted Wannier Charge Centers (WCCs) [31]. Figure 4c shows the determination of the Z_2 invariant with k_x treated as the pumping parameter running from 0 to π for an effective 1D system. Kramers pairs form at k_x = 0 and π, but not elsewhere. Each blue dot represents the center of the *largest gap* between the adjusted WCCs. We see that the gap center jumps down over one WCC, which is odd. Thus Z_2 index is 1, indicating the non-triviality.

Knowing the existence of topological states in BiAg/Si(111)-4×4 surface, we further studies the SHC as obtained from the so-called spin Chern number calculation [32] to characterize the robustness of transverse electrical transport property against temperature perturbations and trivial metallic states, where a wide and stable quantized conductance plateau is desired. The definition of spin Chern number is $C_s = \frac{1}{2\pi}\int_{BZ} d^2\vec{k}\sum_n f_{nk}\Omega_n^s(\vec{k})$ with the Fermi distribution function of f_{nk} and the spin Berry curvature of $\Omega_n^s(\vec{k}) = -2\,\mathrm{Im}\sum_{m\neq n}\frac{\langle\psi_{nk}|j_x|\psi_{mk}\rangle\langle\psi_{mk}|v_y|\psi_{nk}\rangle}{(\varepsilon_{mk}-\varepsilon_{nk})^2}$, here ψ_{nk} is the eigenstate of eigenvalue ε_{nk} of band *n*, j_x is the spin-velocity operator defined as ($s_z v_x + v_x s_z$)/2, s_z and $v_{x/y}$ is the spin operator and the velocity operator, respectively. Figure

4d shows the calculated SHC ($\sigma_{xy}^{SHC} = 2 \times C_s \frac{e}{4\pi}$) as a function of the electron filling. The quantized value of -2×e/4π within the SOC gap above the Fermi level indicates the characteristic transport property of quantum spin Hall (QSH) insulator, which is robust against finite perturbations because of a large non-trivial bulk gap (~71 meV) that cannot be easily closed. Moreover, because the non-trivial Dirac edge states are well isolated from other trivial metallic states below the Fermi level (see Fig. 4b), the TM state also shows a *quasi*-quantized feature with a width of conductance plateau up to ~50 meV, indicating certain degree of robustness against trivial metallic states [33,34].

The robust plateau of the SHC indicates a promising perspective for experimentally measuring the quantized conductivity of non-trivial edge states in BiAg/Si(111)-4×4 surface, similar to that observed in HgTe/CdTe and InAs/GaSb quantum well [6,7], but with large energy gap. The well-developed doping technology based on semiconducting substrates, such as gating that can realize carrier doping with the concentration ranging from 10^{12} to 10^{14} cm^{-2} [35-37], can be taken advantage of to include system with non-intrinsic topological states.

Specifically, for transport experiments and future device application, one needs to dope one electron/hole per unit-cell (doping concentration: 4.83×10^{13} cm^{-2}) to move the Fermi level up/down to the energy range of non-trivial states. Given that the BiAg/Si(111)-4×4 surface is composed of 2D monolayer of BiAg alloy and semiconducting substrate, standard gating technology should be easily applicable to dope this system. Both back gate (V_b) and top gate (V_t) are feasible to reach the desired doping level of ~10^{13} cm^{-2}, as shown in Fig.5a and 5b. This same method has been successfully used to measure the conductance of QSH states in HgTe/CdTe quantum wells, in which the carrier concentration was tuned from *n*- to *p*-type through applying an external gate voltage [6]. Additionally, we would like to discussing other possible doping strategy that is substituting the atom of host material itself, which has been found effective for Bi_2Te_3 [38], Bi_2Se_3 [39], and Bi_2Te_2Se [40]. Phosphorus/boron substituting Si atom of substrate provides a feasible method of realizing doping because they are well-established industrial technologies [41-43]. Moreover, we below that substituting Bi@T_1 with group VI/IV elements can also realize electron/hole doping without disturbing the topological property of BiAg/Si(111)-4×4 surface. The feasibility of such method is based on previous orbital analysis. As we discussed above, the p_{xy} orbitals of Bi@T_4 and Bi@H_3 contribute mainly to the four non-trivial bands near Fermi level, while Bi@T_1 and other atoms have little contributions. Taking tellurium (Te) as an example, our calculations show that Te atom prefers to substituting Bi@T_1 than Bi@T_4 and Bi@H_3 by about 91.8 and 69.6 meV/unit-cell, respectively. The atomic structure of the BiAg/Si(111)-4×4 surface with Bi@T_1 being substituted by Te atom is shown in Fig. S7 [23]. Te atom plays the role of electron doping and moves the Fermi level up to the energy gap of TI state successfully (Fig. 5c), while maintaining the nontrivial topology as characterized by the Dirac-like edge states (Fig. 5d). SHC calculation (Fig. 5e) also confirms the robust transport property of the topological state against atomic substitution.

We note that the system we explore here represents a 2D metal alloy of BiAg on Si(111)-4×4 surface, which is different from that of growing a metal overlayer such as Bi on Au-covered Si surface, such as Au/Si(111)-$\sqrt{3}\times\sqrt{3}$ surface [44] in several important aspects. In our system, Bi atoms sit in a Ruby lattice, while in that system it is a hexagonal or trigonal lattice. Consequently, the resulting topological band structures and underlying formation mechanism are also different.

CONCLUSION

We demonstrate from first-principle calculations that the already-synthesized BiAg/Si(111)-4×4 surface has robust topological nontrivial edge states rising from the p_{xy} orbitals of Bi, which are well decoupled from the other electronic states due to charge transfer and bond formation between BiAg alloy and Si substrate. The topological property is confirmed by calculations of edge states, WCCs, spin Chern number, and analyzed with a minimal effective TB model. Electron doping will transform BiAg/Si(111)-4×4 surface into a 2D TI with a nontrivial gap of 71 meV, corresponding to a temperature up to 819 K for a QSH effect. Hole doping converts BiAg/Si(111)-4×4 surface into a 2D TM, where a finite quantized conductance plateau of ~50 meV is still observable because of the limited interference from the trivial metallic states. Therefore, BiAg/Si(111)-4×4 surface provides a promising material platform for detecting nontrivial topological edge states and investigating its exotic transport properties, and we await future experiments to confirm our theoretical predictions.

ACKNOWLEDGMENT

X.Z. acknowledge financial support from China Postdoctoral Science Foundation Grant (No. 2017M620730). F.L. acknowledge financial support from DOE-BES (No. DE-FG02-04ER46148). M.Z. acknowledge financial support from the National Natural Science Foundation of China (No. 21433006) and the National Key Research and Development Program of China (No. 2016YFA0301200). We also thank Supercomputing Center at NERSC and CHPC at University of Utah for providing the computing resources.

REFERENCE

[1] C. L. Kane and E. J. Mele, Phys. Rev. Lett. **95**, 226801 (2005).
[2] B. A. Bernevig, T. L. Hughes, and S.-C. Zhang, Science **314**, 1757 (2006).
[3] M. Z. Hasan and C. L. Kane, Rev. Mod. Phys. **82**, 3045 (2010).
[4] X.-L. Qi and S.-C. Zhang, Rev. Mod. Phys. **83**, 1057 (2011).
[5] Y. F. Ren, Z. H. Qiao, and Q. Niu, Rep. Prog. Phys. **79**, 066501 (2016).
[6] M. König, S. Wiedmann, C. Brüne, A. Roth, H. Buhmann, L. W. Molenkamp, X.-L. Qi, and S.-C. Zhang, Science **318**, 766 (2007).
[7] I. Knez, R.-R. Du, and G. Sullivan, Phys. Rev. Lett. **107**, 136603 (2011).
[8] F. Yang, L. Miao, Z. F. Wang, M.-Y. Yao, F. Zhu, Y. R. Song, M.-X. Wang, J.-P. Xu, A. V. Fedorov, Z. Sun, G. B. Zhang, C. Liu, F. Liu, D. Qian, C. L. Gao, and J.-F.

Jia, Phys. Rev. Lett. **109**, 016801 (2012).
[9] Z. F. Wang, M.-Y. Yao, W. Ming, L. Miao, F. Zhu, C. Liu, C. L. Gao, D. Qian, J.-F. Jia, and F. Liu, Nat. Commun. **4**, 1384 (2013).
[10] T. Hirahara, G. Bihlmayer, Y. Sakamoto, M. Yamada, H. Miyazaki, S.-I. Kimura, S. Blugel, and S. Hasegawa, Phys. Rev. Lett. **107**, 166801 (2011).
[11] Y. Lu, W. Xu, M. Zeng, G. Yao, L. Shen, M. Yang, Z. Luo, F. Pan, K. Wu, T. Das, P. He, J. Jiang, J. Martin, Y. P. Feng, H. Lin, and X.-S. Wang, Nano Lett. **15**, 80 (2015).
[12] G. Bian, Z. Wang, X. X. Wang, C. Xu, S. Xu, T. Miller, M. Z. Hasan, F. Liu, and T. C. Chiang, ACS Nano **10**, 3859 (2016).
[13] M. Zhou, W. Ming, Z. Liu, Z. Wang, P. Li, and F. Liu, P. Natl. Acad. Sci. USA **111**, 14378 (2014).
[14] F. Reis, G. Li, L. Dudy, M. Bauernfeind, S. Glass, W. Hanke, R. Thomale, J. Schäfer, and R. Claessen, Science **357**, 287 (2017).
[15] P. Li, M. Zhou, L. Z. Zhang, Y. H. Guo, and F. Liu, Nanotechnology **27**, 095703 (2016).
[16] Z. F. Wang, H. Zhang, D. Liu, C. Liu, C. Tang, C. Song, Y. Zhong, J. Peng, F. Li, C. Nie, L. Wang, X. J. Zhou, X. Ma, Q. K. Xue, and Feng Liu, Nat. Mater. **15**, 968 (2016).
[17] N. V. Denisov, E. N. Chukurov, Y. V. Luniakov, O. A. Utas, S. G. Azatyan, A. A. Yakovlev, A. V. Zotov, and A. A. Saranin, Surf. Sci. **623**, 17 (2014).
[18] G. Kresse and J. Furthmüller, Phys. Rev. B **54**, 11169 (1996).
[19] G. Kresse and J. Hafner, Phys. Rev. B **48**, 13115 (1993).
[20] A. A. Mostofi, J. R. Yates, Y.-S. Lee, I. Souza, D. Vanderbilt, and N. Marzari, Comput. Phys. Commun. **178**, 685 (2008).
[21] J. P. Perdew, K. Burke, and M. Ernzerhof, Phys. Rev. Lett. **77**, 3865 (1996).
[22] G. Kresse and D. Joubert, Phys. Rev. B **59**, 1758 (1999).
[23] See Supplemental Materials at http:// contain the illustration of position for Bi@T_1, Bi@T_4, and Bi@H_3, projected band structures of freestanding BiAg alloy, the variation of band structure of BiAg/Si(111)-4×4 surface when manually modifying SOC strength, details of our minimal effective TB model, the plane-averaged electrostatic potential energy and charge density, as well as the atomic structure of BiAg/Si(111)-4×4 surface with Bi@T_1 being substituted by Te atom.
[24] X. Hu, M. Kargarian, and G. A. Fiete, Phys. Rev. B **84**, 155116 (2011).
[25] W. Ming, Z. F. Wang, M. Zhou, M. Yoon, and F. Liu, Nano Lett. **16**, 404 (2016).
[26] C. R. Ast, J. Henk, A. Ernst, L. Moreschini, M. C. Falub, D. Pacilé, P. Bruno, K. Kern, and M. Grioni, Phys. Rev. Lett. **98**, 186807 (2007).
[27] C. Wu, Phys. Rev. Lett. **101**, 186807 (2008)
[28] Z. Liu, Z.-F. Wang, J.-W. Mei, Y.-S. Wu, and F. Liu, Phys. Rev. Lett. **110**, 106804 (2013)
[29] M. P. L. Sancho, J. M. L. Sancho, J. M. L. Sancho, and J. Rubio, J. Phys. F: Metal Physics **15**, 851 (1985).
[30] L. Fu and C. L. Kane, Phys. Rev. B **74**, 195312 (2006).
[31] A. A. Soluyanov and D. Vanderbilt, Phys. Rev. B **83**, 235401 (2011).

[32] D. N. Sheng, Z. Y. Weng, L. Sheng, and F. D. M. Haldane, Phys. Rev. Lett. **97**, 036808 (2006).
[33] A. Junck, K. W. Kim, D. L. Bergman, T. Pereg-Barnea, and G. Refael, Phys. Rev. B **87**, 235114 (2013).
[34] Y.-Y. Zhang, M. Shen, X.-T. An, Q.-F. Sun, X.-C. Xie, K. Chang, and S.-S. Li, Phys. Rev. B **90**, 054205 (2014).
[35] K. Ueno, S. Nakamura, H. Shimotani, A. Ohtomo, N. Kimura, T. Nojima, H. Aoki, Y. Iwasa, and M. Kawasaki, Nat. Mater. **7**, 855 (2008).
[36] K. S. Novoselov, A. K. Geim, S. V. Morozov, D. Jiang, Y. Zhang, S. V. Dubonos, I. V. Grigorieva, and A. A. Firsov, Science **306**, 666 (2004).
[37] A. Das, S. Pisana, B. Chakraborty, S. Piscanec, S. K. Saha, U. V. Waghmare, K. S. Novoselov, H. R. Krishnamurthy, A. K. Geim, A. C. Ferrari, and A. K. Sood, Nat. Nanotechnol. **3**, 210 (2008).
[38] Y. L. Chen, J. G. Analytis, J.-H. Chu, Z. K. Liu, S.-K. Mo, X. L. Qi, H. J. Zhang, D. H. Lu, X. Dai, Z. Fang, S. C. Zhang, I. R. Fisher, Z. Hussain, and Z.-X. Shen, Science **325**, 178 (2009).
[39] Y. S. Hor, A. Richardella, P. Roushan, Y. Xia, J. G. Checkelsky, A. Yazdani, M. Z. Hasan, N. P. Ong, and R. J. Cava, Phys. Rev. B **79**, 195208 (2009).
[40] Z. Ren, A. A. Taskin, S. Sasaki, K. Segawa, and Y. Ando, Phys. Rev. B **85**, 155301 (2012).
[41] E. Baek, T. Rim, J. Schütt, C.-K. Baek, K. Kim, L. Baraban, and G. Cuniberti, Nano Lett. **17**, 6727 (2017).
[42] E. A. Ekimov, V. A. Sidorov, E. D. Bauer, N. N. Mel'nik, N. J. Curro, J. D. Thompson, and S. M. Stishov, Nature **428**, 542 (2004).
[43] B. Slomski, G. Landolt, G. Bihlmayer, J. Osterwalder, and J. Hugo Dil, Sci. Rep. **3**, 1963 (2013).
[44] B. Huang, K.-H. Jin, H. L. Zhuang, L. Zhang, and F. Liu, Phys. Rev. B **93**, 115117 (2016).

Figures

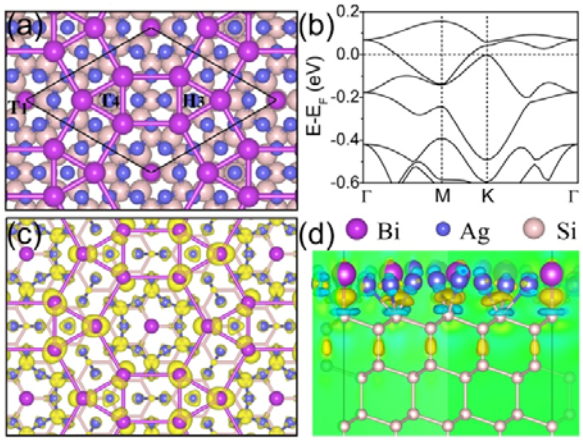

Figure 1. (Color online) (a) Schematic representation of BiAg/Si(111)-4×4 surface with the unit-cell indicated by a rhombus. Only the Si atoms of top bilayer were plotted for clarity. Bi@T_4 and Bi@H_3 are bonded together to highlight the Ruby lattice pattern. (b) Band structure of BiAg/Si(111)-4×4 surface without considering SOC. The Fermi level is set to zero. (c) The charge density distribution of the four isolated bands at all the K points sampled in BZ. (d) Illustration of charge transfer between the BiAg alloy and the silicon substrate, which is calculated by subtracting the charge density of freestanding BiAg alloy and surface-exposed silicon substrate from the total charge density of BiAg/Si(111)-4×4 surface. The yellow (blue) isosurfaces indicate the increase (decrease) of electronic density.

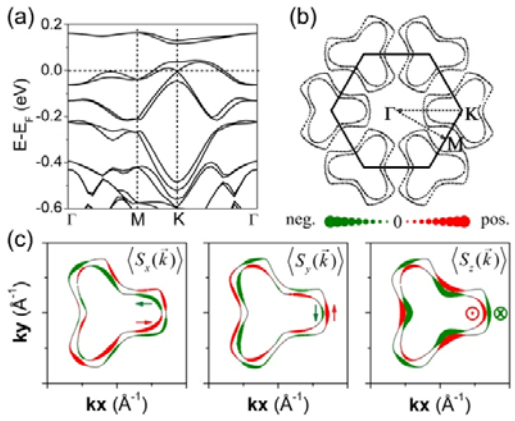

Figure 2. (Color online) (a) SOC included band structure and (b) Fermi surface contour of BiAg/Si(111)-4×4 surface. The Fermi surface contour formed by the Dirac cone near the Fermi level was very small and hence not plotted. (c) The spin polarization $\langle s_x(\vec{k})\rangle$, $\langle s_y(\vec{k})\rangle$, $\langle s_z(\vec{k})\rangle$ at the Fermi surface contour. Red (green) color represents parallel (anti-parallel) to the projected direction of *x*, *y*, and *z*, respectively.

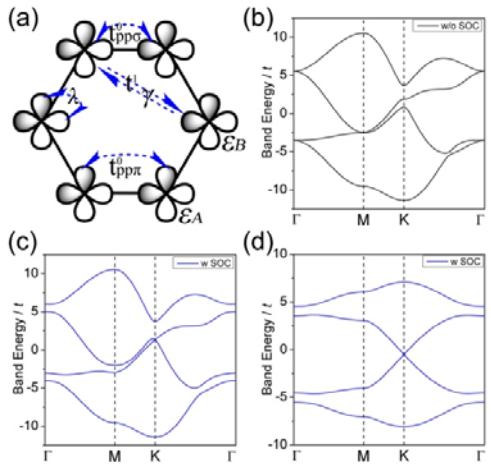

Figure 3. (Color online) (a) Schematic of the p_{xy} orbitals TB model on honeycomb lattice with the illustrations of neighbor hopping ($t^0_{pp\sigma}$, $t^0_{pp\pi}$) and second-neighbor hopping (t^l, γ). λ indicates the intrinsic SOC strength between p_x and p_y orbitals. ε_A and ε_B are the onsite energy of the p_{xy} orbitals on different sub-lattice. (b, c) Band dispersions of the TB model (b) without and (c) with considering SOC. (d) The typical four topological bands evolved from the bands in figure (c) by removing the perturbations of surrounding Ag atoms away.

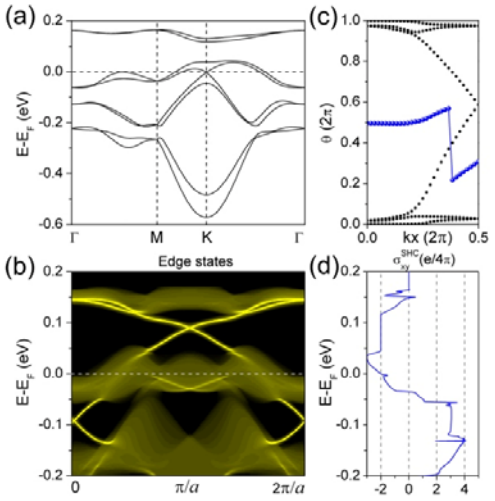

Figure 4. (Color online) (a) The Wannier-interpolated band structure and (b) the *semi*-infinite edge states of BiAg/Si(111)-4×4 surface with considering SOC. (c) Evolutions of WCCs versus k_x at the nontrivial gap above the Fermi level. Blue dots mark the center of the *largest gap* between adjusted WCCs. (d) The SHC as a function of electron filling.

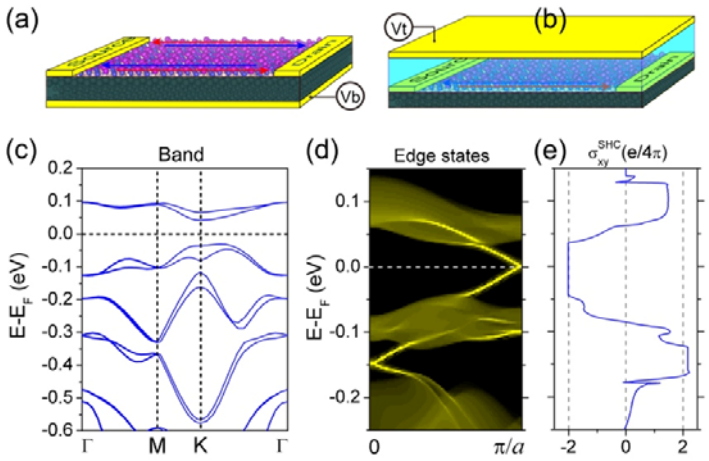

Figure 5. (Color online) A schematic illustration of the experimental setup for realizing electron/hole doping by using (a) back gate (V_b) and (b) top gate (V_t) voltage. (c) Band structure, (d) *semi*-infinite edge states, and (e) calculated SHC of BiAg/Si(111)-4×4 surface with Bi@T_1 being substituted by Te atom. The Fermi level is set at the middle of non-trivial gap.